Volume 11
Number 2
February 2026
Pages 317–596

Nanoscale Horizons

The home for rapid reports of exceptional significance in nanoscience and nanotechnology

rsc.li/nanoscale-horizons

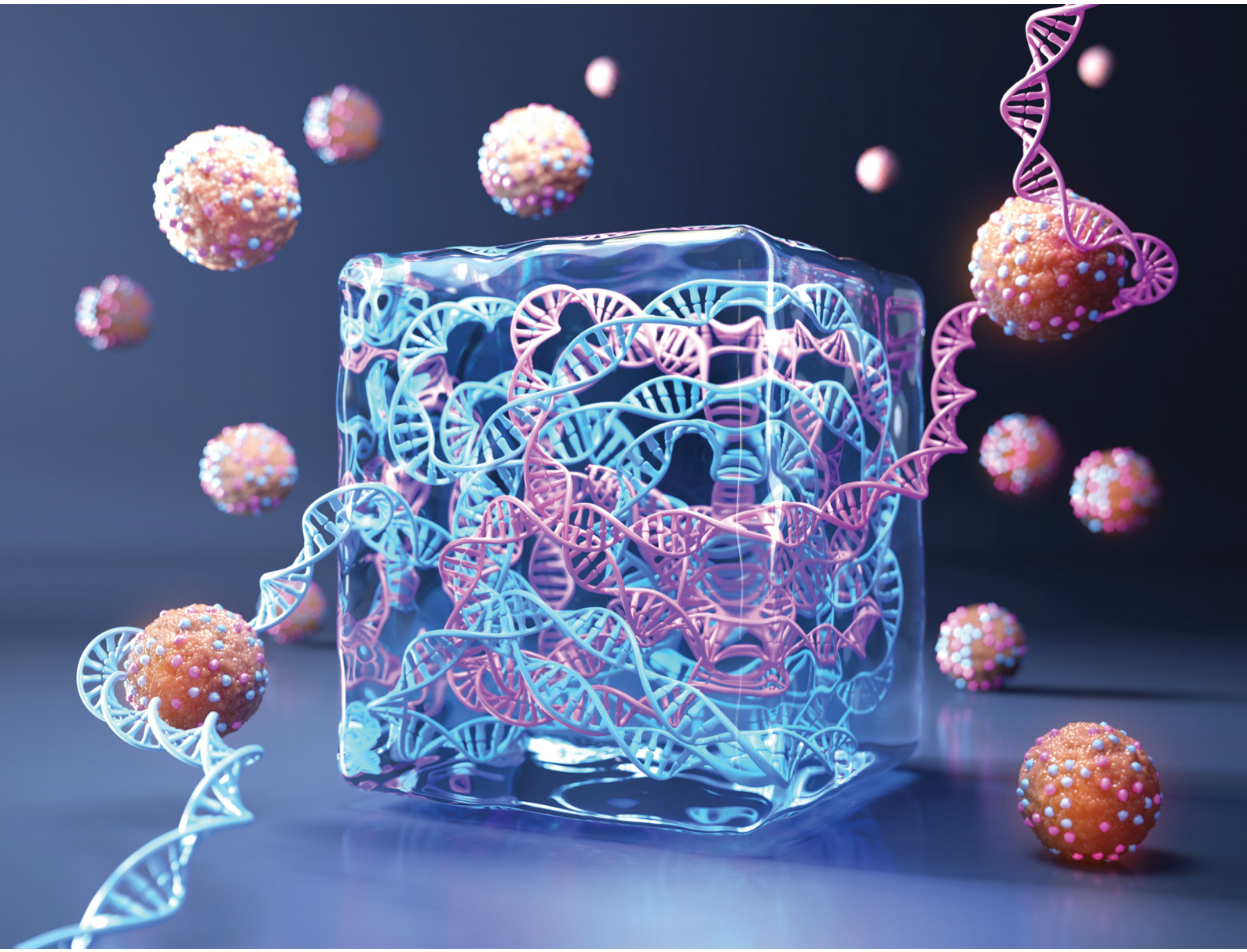

ISSN 2055-6756

ROYAL SOCIETY OF CHEMISTRY

COMMUNICATION
Young Hoon Roh *et al.*
Cell instructive hydrogels functionalized with polymerized DNA nanostructures

NCNST

Nanoscale Horizons

ROYAL SOCIETY OF CHEMISTRY

COMMUNICATION

View Article Online
View Journal | View Issue

Cite this: *Nanoscale Horiz.*, 2026, **11**, 469

Received 22nd July 2025,
Accepted 4th November 2025

DOI: 10.1039/d5nh00521c

rsc.li/nanoscale-horizons

Cell instructive hydrogels functionalized with polymerized DNA nanostructures

Hee Yeon Kim,† Young Min Kim,† Keonwook Nam, Kyungjik Yang, Joohyun Oh, Su-Min Han and Young Hoon Roh *

Novel hyaluronic acid hydrogels functionalized with polymerized DNA nanostructures using rolling circle amplification were developed. These hydrogels exhibited enhanced cell attachment and proliferation through functional DNA-mediated interactions. The system maintained favorable physicochemical properties and enhanced interactions with biological interfaces, demonstrating potential for advanced 3D cell culture applications.

New concepts

This study presents a novel strategy for engineering functional hydrogels by incorporating polymerized functional DNA nanostructures synthesized using rolling circle amplification (RCA). Unlike conventional approaches that rely on chemically modifying short aptamers or ligands, our approach utilizes RCA to generate high-molecular-weight, repetitive functional DNA nanostructures that self-assemble and physically entangle within hydrogel matrices. This approach enables dense and stable integration of bioactive moieties without requiring covalent crosslinking or toxic chemical modifications. Our approach stands out for its ability to simultaneously enhance both the structural retention and functional performance of DNA nanostructures, thereby promoting cell attachment and proliferation within 3D culture systems. By demonstrating that DNA nanostructure functionality can be amplified and stabilized through polymerization, we introduce a new framework for designing biomimetic matrices with tunable biochemical cues. This insight advances the field of nanobiomaterials by bridging nucleic acid nanotechnology and 3D tissue engineering, offering a versatile platform for investigating cell–matrix interactions and developing next-generation scaffolds for regenerative medicine.

Introduction

Given recent advances in biomaterials, regenerative medicine, and biopharmaceutics, evaluation methodology has become more advanced and sophisticated.[1] For example, due to the ethical, scientific, and regulatory requirements of animal experiments, development of cell culture systems mimicking the *in vivo* environment has become increasingly important. Current conventional two-dimensional (2D) cell culture platforms, which rely on cells adhered to a flat surface, cannot fully replicate the native microenvironments of physiological systems.[2,3] Three-dimensional (3D) cell culture presents a much more accurate alternative to the 2D cell culture that can recapitulate complex interplays of biological interfaces.[4] To mimic various biological tissues including the vasculature, nerve system, and gastrointestinal tract, microfabrication tools such as organ-on-a chip, 3D-printing, and hydrogels have been developed.[5–8] Hydrogels can most accurately represent the cell microenvironment owing to their biocompatibility and mechanically soft and flexible properties.[9–11] The high-water content of hydrogels is similar to that of the physiological environment, and unlike a flat surface, they can structurally support three-dimensional space and allow cell-to-cell interactions. Moreover, the adjustable pore structure and stiffness of hydrogels reinforce their feasibility as a 3D support.[12,13] Despite these advantages, hydrogels lack the instructive and interactive components of the native extracellular matrix (ECM), which interacts with cells *via* various functional molecules including fibronectins, proteoglycans, and glycosaminoglycans.[14,15] In this regard, developing hydrogels that can mimic these functional ECM interactions or incorporate specific biological molecules is essential for developing advanced 3D cell culture systems.

Nucleic acid-based nanostructures have been widely studied for enhancing cell–hydrogel interactions. An aptamer is a representative functional DNA nanostructure known for its ability to interact with biological molecules (*e.g.* ATP, growth factors, hormones, and receptors) that comprises many nucleotides, generally approximately 20 nt.[16,17] Specific aptamer sequences spontaneously assemble into DNA nanostructures. The dynamic structure of aptamers enables them to bind to their targets after structural recognition in a process that is similar to that of antibody–antigen binding.[18] Moreover, aptamers not only target membrane proteins, but also induce signal transduction and promote changes in cellular behavior, such as

Department of Biotechnology, College of Life Science and Biotechnology, Yonsei University, 50 Yonsei-ro, Seodaemun-gu, Seoul, 03722, South Korea.
E-mail: yr36@yonsei.ac.kr
† These authors contributed equally to this work.

proliferation.[19–21] Wang's group reported aptamer-based cell recruitment on 2D surfaces and 3D hydrogels.[22–24] They demonstrated that an aptamer conjugated on a hydrogel could recruit cells *via* direct cell-to-aptamer or growth factor-mediated interactions. Our previous work also demonstrated optimization of aptamer functionalization for 3D cell culture by investigating the effects of aptamer density, isotropicity, and structures on homogeneity and cell behaviors.[25] Despite the importance of spatial control of functional nanostructures, efficient conjugation strategies are required as loading capacity and density are limited. Rolling circle amplification (RCA) is a powerful DNA nanotechnology tool that enables repeated replication of defined sequences.[26,27] RCA fabricates very long DNA strands with over 100 copies of the original template which can be used as native hydrogels on their own self-assembled formulate with magnesium pyrophosphate or to extract long strands of DNA for various applications.[28] Yang's group developed polymerized aptamer nanostructures for sequestration of a desired cell type from multiple cell populations for cell fishing.[29,30] Roh's group demonstrated the importance of stoichiometry and physicochemical properties of a replicated DNA hydrogel for sequence-based function.[31] Based on this, we inferred that the use of polymerized functional DNA nanostructures generated by RCA offers two key advantages: enhancement of both the functionality and stability of DNA nanostructures, and loading of sufficient functional moieties onto hydrogels with more complex and elongated architectures.

In this study, we adopted RCA as a 3D cell culture hydrogel platform based on the following hypotheses: (1) RCA replicates short DNA sequences and converts them into long polymerized DNA, resulting in DNA networks comprised of desired nanostructures; (2) the molecular weight of polymerized DNA nanostructures is large enough for tight incorporation into hydrogel matrices through noncovalent interactions and physical entanglements without the need for any nonbiocompatible chemicals; and (3) the repetition of DNA nanostructures increases the likelihood of hydrogel matrix–cell membrane protein production, leading to improved cellular attachment and signal transduction. As a proof of concept, two types of aptamers—anti-nucleolin and anti-FGFR1—were selected as functional moieties to promote DNA nanostructures-based cell attachment and proliferation, respectively (Fig. 1A). We chose hyaluronic acid (HA), a major component of the ECM, as a supporting hydrogel matrix with methacrylate modification for hydrogel network fabrication (Fig. 1B). The changes in physicochemical and rheological properties attributed to the adoption of polymerized DNA nanostructures were evaluated. Finally, we compared the cell-instructive effectiveness of DNA nanostructure polymerization to non-polymerized aptamers using cell attachment and proliferation assay (Fig. 1C).

Results and discussion

Validation of functional DNA nanostructures

Among various DNA nanostructures, two types of DNA nanostructures, AS1411 and bFGF aptamers, were selected as proof-of-concept to evaluate matrix–cell interactions in hydrogels. AS1411 is a well-known aptamer structure, which binds with nucleolin on the cytosolic membrane.[32–34] In previous studies, AS1411-mediated cell attachment was evaluated in both 2D and 3D platforms.[31] The bFGF aptamer sequence binds to FGFR1 on the cell surface and triggers phosphorylation of the downstream Erk pathway and resulting in cell proliferation.[35,36] Therefore, we examined the sequence-mediated effects on cell attachment and proliferation.

To determine appropriate nucleolin-positive cell lines, we validated the binding level of a 6-carboxy-fluorescein (FAM)-labelled AS1411 aptamer on NIH-3T3, HeLa, and A-204 cells using flow cytometry (Fig. S1). The fluorescence intensities of 20 nM FAM-labelled AS1411-treated NIH-3T3, HeLa, and A-204 showed 3.0-, 8.5-, and 10.5-fold increases, respectively, compared with non-treated controls. The binding affinity of AS1411 was superior in the A-204 cell line, implying high expression of nucleolin on the cell surface. Therefore, the AS1411 aptamer and A-204 cell line were selected as appropriate models for evaluating the interaction between the aptamer and cells in the hydrogel.

As A-204 cells are known to express the bFGF receptor, bFGF aptamer-mediated proliferation enhancement was evaluated in A-204 cells. Compared with non-treated cells, A-204 cells treated with 160 nM bFGF aptamer showed significantly enhanced proliferation on day 5, similar to that of cells treated with 160 nM nonspecific (NS) DNA (Fig. S2). Hence, we identified appropriate cell lines for both cell attachment and proliferation studies.

Polymerization of functional DNA nanostructures

Isothermal replication of these functional DNA nanostructures was performed using RCA for three purposes: (1) enhanced accumulation of functional DNA nanostructures with repeated nanostructures, (2) increased loading efficiency on the hydrogel through longer and more complex structures, and (3) enhanced physiological stability owing to decreased enzymatic accessibility (Fig. 2A). For RCA, we designed two circular DNAs, each encoding its respective aptamer (Fig. S3 and Table S1).

RCA products exhibited fetal-like spherical structures, composed of C, N, O, P, and Mg atoms (Fig. 2B and Fig. S4). The crystalline structure of the RCA product was magnesium pyrophosphate (MgPPi) crystals formed *via* electrostatic interaction between Mg^{2+} from the reaction buffer and pyrophosphate produced as a byproduct of DNA replication.[37] In the EDS data, C, N, O, and P indicate the presence of DNA, while O, Mg, and P indicate the presence of MgPPi crystals. N is uniquely present in DNA and not in MgPPi, serving as an indicator of DNA localization, while Mg primarily reflects the presence of MgPPi crystals. The distribution of N and Mg throughout the particles suggests that DNA and MgPPi are well-integrated during the polymerization process. Our previous findings suggested that the presence of MgPPi crystals hindered DNA functionalities.[27] Therefore, to enhance DNA functionalities, ethylenediaminetetraacetic acid (EDTA) was introduced to the RCA product as a Mg^{2+} chelator to disrupt MgPPi crystals, resulting in amorphous, polymerized functional DNA nanostructures (pFDN) (Fig. 2C). The polymerization and decomplexation with MgPPi were also revealed in gel

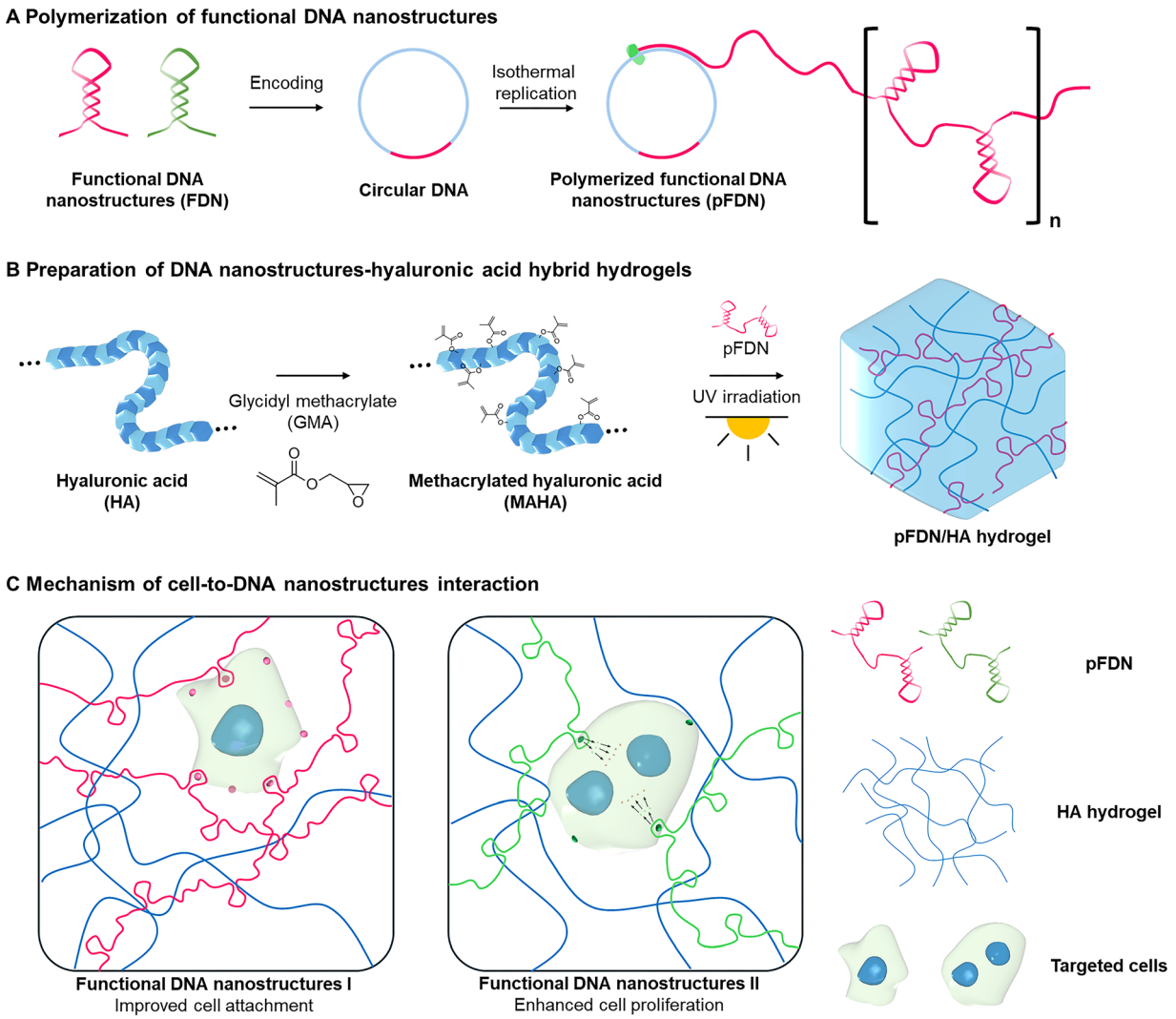

Fig. 1 Synthetic scheme of polymerized functional DNA nanostructures–hyaluronic acid hybrid hydrogels. (A) Isothermal polymerization of functional DNA nanostructures. (B) Modification of hyaluronic acid and UV-triggered hydrogels functionalized with polymerized DNA nanostructures synthesis. (C) Mechanism of action of two types of polymerized DNA nanostructures-mediated cell functions within the hydrogels. FDN, functional DNA nanostructures; pFDN, polymerized FDN; HA, hyaluronic acid; and MAHA, methacrylated HA.

electrophoresis (Fig. 2D). Monomeric FDN (mFDN) showed a highly shifted band in gel electrophoresis, whereas the RCA product rarely shifted, with most residues being trapped in the loading well. When EDTA was applied, smearing from the well was observed, indicating de-complexed DNA strands. The relative migration (R_f) against FDN was 0.04 and 0.4 in the RCA product and pFDN, respectively. The estimated molecular weight of pFDN is approximately 5.8 MDa (Fig. S5). The structural characteristics of pFDN and thermal stability of aptamer structures were analyzed using circular dichroism (CD) (Fig. S6). Strong peaks appeared in the CD spectra of both mFDN and pFDN because these 3D aptamer structures contain right-handed double helix structures. When the temperature was increased to 90 °C, the strong peaks were diminished, as the FDN was denatured and the 3D aptamer structure was disrupted.

The effect of polymerization on the physiological stability following incubation with serum and DNase was evaluated using gel electrophoresis (Fig. 2E and Fig. S7). The serum stability of mFDN and pFDN was evaluated based on their half-lives, which were estimated to be approximately 1.6 h for mFDN and 36 h for pFDN. Notably, the half-life of pFDN was approximately 23 times longer than that of mFDN. Regarding DNase stability, mFDN was degraded within 8 h in the presence of 25 U mL^{-1} DNase, whereas 85% of pFDN was maintained. The polymerization of DNA nanostructures allowed the formation of more complex structures, interfering with enzyme access *via* steric hindrance. Enhancement of pFDN functionalities was validated using a bFGF aptamer-mediated cell proliferation assay (Fig. 2F). The proliferation rate of A-204 cells after treatment with 160 nM mFDN (bFGF) and pFDN (bFGF) was quantified using a Cell Counting Kit-8 assay. After culturing for 7 d following pFDN (bFGF) treatment, the proliferation rate was 1.7-fold higher than that in non-treated cells. These results suggested that bFGF nanostructures were correctly formed after polymerization, and

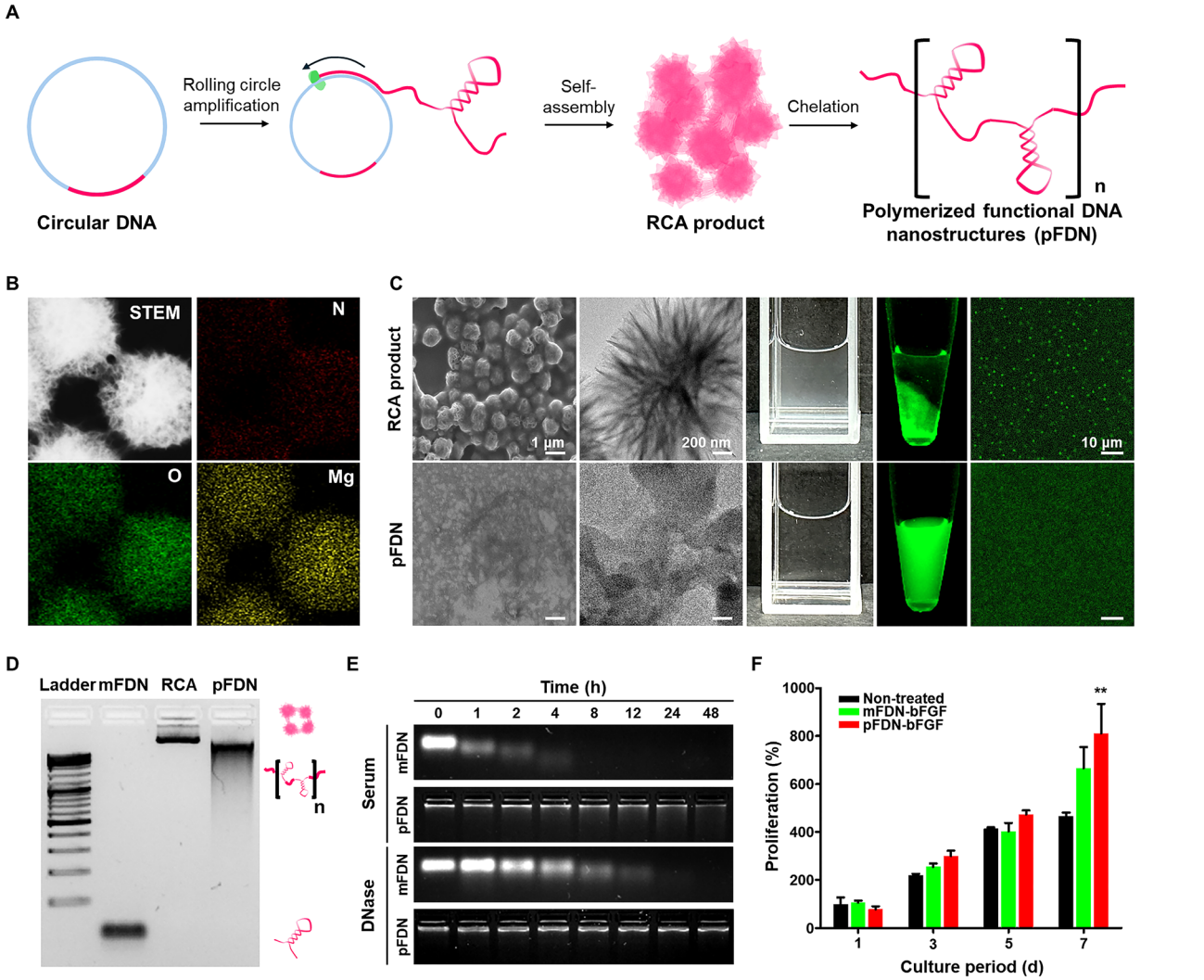

Fig. 2 Synthesis and characterization of functional DNA nanostructures. (A) Synthetic scheme of pFDN. (B) EDS analysis of the RCA product. (C) SEM, TEM, digital, fluorescence, and CLSM images of the RCA product and pFDN. (D) Gel electrophoresis images of mFDN, RCA product, and pFDN (1% agarose gel, running on 100 V for 30 min). (E) Gel electrophoresis images of FDN under serum and DNase incubation (2% agarose gel, running on 100 V for 30 min). (F) Comparison of cell proliferation of A-204 cells treated with 160 nM mFDN-bFGF and 160 nM pFDN-bFGF. Data are presented as the mean ± SD (n = 3); the differences between experimental and control groups were assessed using Scheffe's *post hoc* test. *$p < 0.05$, **$p < 0.01$, and ***$p < 0.001$ *versus* the non-treated group. pFDN, polymerized functional DNA nanostructures; RCA, rolling circle amplification; SEM, scanning electron microscopy; TEM, transmission electron microscopy; CLSM, confocal laser scanning microscopy; EDS, energy-dispersive X-ray spectroscopy; and mFDN, monomeric functional DNA nanostructures.

the superior thermodynamic and physiological stability contributed to the enhanced proliferation rate. Overall, pFDN was synthesized *via* RCA and EDTA chelation. The polymerized nanostructures exhibited higher thermal and enzymatic stabilities. The functionality of pFDN was enhanced in the bFGF-mediated cell proliferation assay. These results suggested that polymerization enhances the functionalities of DNA nanostructures.

Synthesis of polymerized DNA nanostructures hybrid hydrogels

Hyaluronic acid (HA) was selected as the matrix for incorporating the functional DNA nanostructures. Although various matrices have been utilized for hybridizing DNA into hydrogels, HA was chosen for this study for the following reasons: (1) HA is a major component of the extracellular matrix (ECM) and is inherently biocompatible. (2) It does not exhibit strong interactions (*e.g.*, electrostatic interactions) with DNA, thereby minimizing any interference with DNA-based functions.

Furthermore, we avoided chemical hybridization of HA and DNA, which could potentially hinder the formation of functional DNA nanostructures. We utilized the long-chain structures of the RCA product, allowing the incorporation of DNA into the HA matrix through physical entanglement.[38] To incorporate synthesized pFDN, HA was modified with methacrylate and reacted with glycidyl methacrylate under basic conditions (Fig. S8). The degree of substitution of methacrylate was approximately 0.6, as calculated using NMR (Fig. S9). The methacrylated HA (MAHA) showed negligible cytotoxicity (Fig. S10). As the reaction time is short and relatively low concentrations of additives (approximately 0.05%) are required, photocrosslinking was chosen for gelation of MAHA (Fig. S11). To optimize the gelation conditions of HA, both the

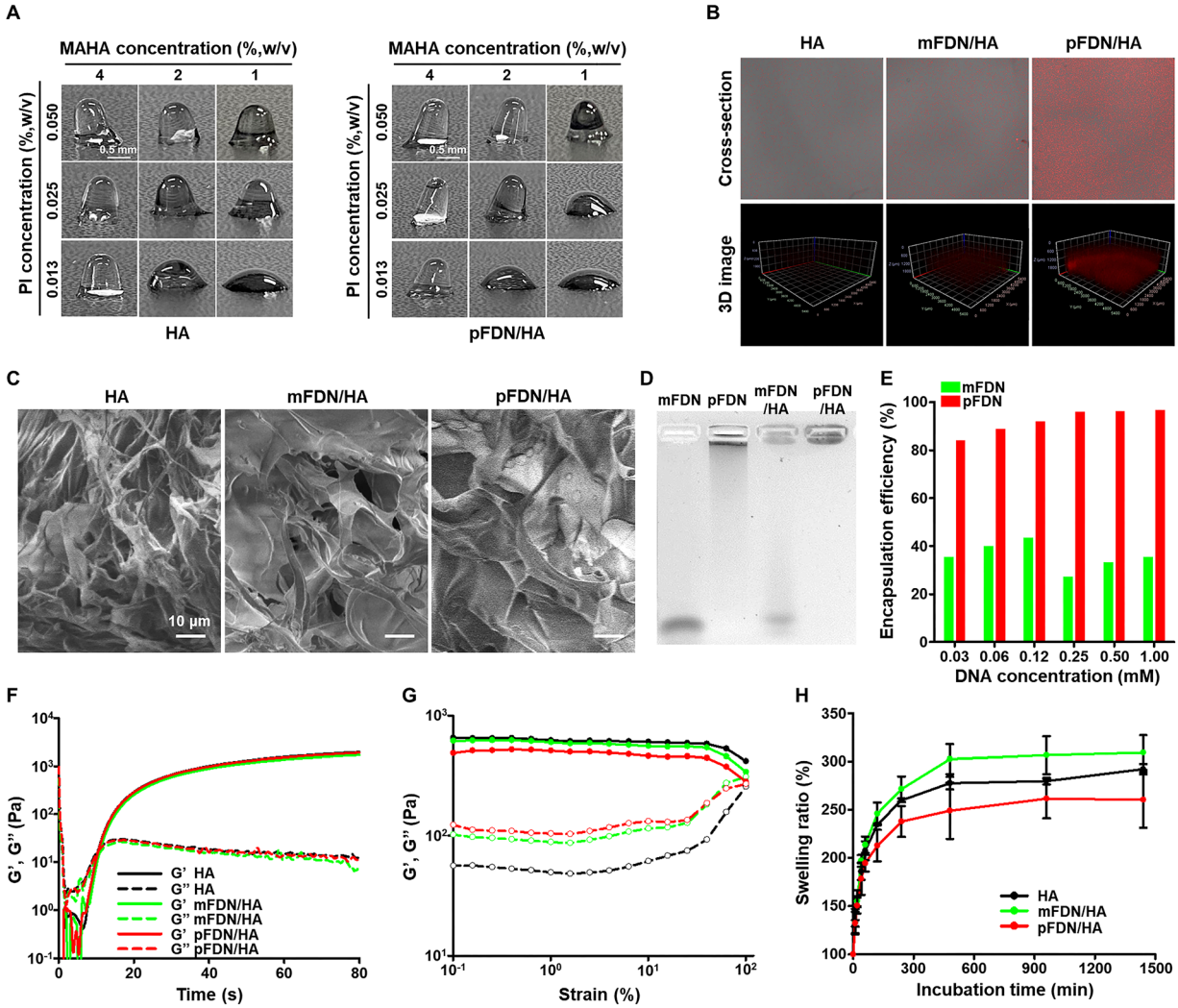

Fig. 3 Synthesis and characterization of the functional DNA nanostructures–hyaluronic acid hybrid hydrogels. (A) Gelation of HA and pFDN/HA with varying HA and PI concentration. (B) 3D stacking images of HA, mFDN/HA, and pFDN/HA gels measured by CLSM. DNA of each hydrogel is stained with GelRed, indicating red fluorescence. (C) SEM images of HA, mFDN/HA, and pFDN/HA. (D) Electrophoresis images of mFDN, pFDN, mFDN/HA, and pFDN/HA hydrogels. (E) Encapsulation efficiency of mFDN and pFDN after gelation with HA, quantified from gel electrophoresis images. (F) Time sweep rheological analysis of HA, mFDN/HA, and pFDN/HA with UV irradiation (1000 mW cm^{-2}). (G) Amplitude sweep rheological analysis of HA, mFDN/HA, and pFDN/HA. (H) Swelling ratio of HA, mFDN/HA, and pFDN/HA. Data are presented as the mean ± SD (n = 3). HA, hyaluronic acid; FDN, functional DNA nanostructures; mFDN, monomeric FDN; pFDN, polymerized FDN; CLSM, confocal laser scanning microscopy; and SEM, scanning electron microscopy.

MAHA and photoinitiator (PI) concentrations were adjusted. Gelation of MAHA was successfully achieved at HA concentrations of 2% and 4% (Fig. 3A). Although HA was crosslinked at all PI concentrations, 0.05% PI was selected considering its toxicity, gel stability in PBS, and rheological properties (Fig. S12 and S13). Moreover, regardless of the presence of pFDN, the gelation results were similar with varying HA and PI concentrations.

To evaluate the incorporation of FDN on the hydrogels, confocal laser scanning microscopy was used after FDN staining using a GelRed DNA-specific dye. Although the HA showed only noise signals, mFDN- and pFDN-containing hydrogels showed significant red fluorescence signals (Fig. 3B). In both hydrogels, the fluorescence was evenly distributed throughout the hydrogel. Because the initial mass concentration was the same in both gels, the differences in intensity indicated the high encapsulation efficiency of pFDN on the hydrogel matrix. Moreover, in terms of DNA damage, we previously validated the feasibility of using DNA nanostructures for photocrosslinking. Matrix components such as PEG were shown to preserve DNA strands, and we believe that HA played a similar protective role in the current study.[25,39,40] In summary, mFDN and pFDN had a minimal effect on the methacrylate group-mediated photocrosslinking, and the nanostructures were successfully incorporated into the hydrogels.

Physicochemical properties of polymerized DNA nanostructures hybrid hydrogels

To verify the effects of FDN introduction, various physicochemical analyses were conducted. In the SEM morphological characterization, all hydrogels, HA, mFDN/HA, and pFDN/HA gels,

exhibited comparable morphology (Fig. 3C). All hydrogels exhibited similar shapes, with no significant differences in the average pore size of 53.2 ± 10.6, 53.15 ± 13.6, and 51.3 ± 11.0 nm, respectively. Because the cell culture studies were conducted after freeze–thaw treatment, further morphological investigation was conducted. Despite the freeze-thawing process, the pore size and cross-sectional structures of the hydrogels were not different (Fig. S14 and S15).

Comparison of the encapsulation efficiency of mFDN and pFDN was performed using gel electrophoresis. mFDN and pFDN were loaded onto the well as solution formulations, whereas mFDN/HA and pFDN/HA were loaded as whole hydrogels. The FDN showed a rapid electrophoretic shift (Fig. 3D). For the mFDN/HA gel, most of the intensity after electrophoresis appeared at a shifted position, nearly identical to that of mFDN, while the rest of the intensity was observed in the loading well. This suggested that the encapsulated DNA appeared in the well and the unencapsulated DNA appeared in the same region of the mFDN. When the pFDN was monitored, smearing from the well was observed. After hybridization with HA, the pFDN/HA gel showed a single band that remained on the well. For further quantification, we examined the encapsulation efficiency from the gel electrophoresis with varying fortified mFDN and pFDN concentrations, which revealed that the polymerization of FDN drastically increased the encapsulation efficiency (Fig. 3E and Fig. S16). The calculated encapsulation efficiency of pFDN was over 80% across all fortified concentrations, whereas that of mFDN was less than 40% across all initial fortified concentrations.

From the perspective of kinetics, we tracked the rheological change during UV illumination to investigate the intersection time of G' and G'', that is, the sol–gel transition point (Fig. 3F). The delayed G'–G'' intersection times for HA, mFDN/HA, and pFDN/HA gels were 10.5, 10.8, and 10.5 s, respectively. No significant difference in the crosslinking kinetics was observed, suggesting that the mFDN and pFDN rarely interfere with the photocrosslinking reaction, consistent with the previous results. In the rheological properties, both mFDN/HA and pFDN/HA gels showed decreased G' and increased G'' compared with those of the HA gel (Fig. 3G), which may be explained by the high loss modulus properties of DNA. Despite decreased storage moduli, the complex moduli were similar for all hydrogels, suggesting that no significant difference in the material properties in the subsequent cell culture applications would be observed. Interestingly, swelling ratio results for hydrogels with mFDN and pFDN showed unexpected differences (Fig. 3H). Compared with the HA gel, the swelling ratio of the mFDN/HA gel was increased, probably because of the noncrosslinked portion of the hydrogel. However, in the pFDN-containing hydrogel, the swelling ratio decreased with respect to the pFDN concentration (Fig. S17). We attributed this phenomenon to the construction of a quasi-interpenetrating network between the HA network and pFDN.[41,42] Compared with mFDN, pFDN is more likely to form inter-molecular networks owing to the higher degree of polymerization. Moreover, distinct from other general polymers, pFDN is rationally designed to self-assemble with inter- and intra-molecular structures. We inferred that this change in the swelling ratio was an inherent characteristic of pFDN. In summary, the hybridization of FDN did not significantly affect the hydrogel properties. pFDN demonstrated much higher encapsulation efficiency and the decrease in the swelling ratio could be attributed to the formation of a quasi-interpenetrating network.

Evaluation of cell instructive function from encapsulated DNA nanostructures

To evaluate the DNA sequence-mediated functionality in the hydrogel-based 3D cell culture model, we assessed cell attachment efficiency on the hydrogel surface mediated by the AS1411 sequence. From optical microscopy images, both mFDN-AS1411/HA and pFDN-NS/HA gels showed similar cell attachment levels to that of the HA gel, whereas a significantly higher number of cells was observed on the pFDN-AS1411/HA gel (Fig. 4A). Fluorescent microscopy images also confirmed that enhanced cell attachment in the pFDN-AS1411/HA gel was concentration-dependent (Fig. 4B). Cell attachment ability showed a non-linear response to increasing pFDN concentrations (AS1411), with a distinct optimal concentration.

In quantification analyses, the cell attachment ability of the pFDN-AS1411/HA gel was approximately 3.5-fold higher than those of HA, mFDN-AS1411/HA, and pFDN-NS/HA gels (Fig. 4C). These results suggested that both factors, the polymerization degree of nanostructures, and the functional sequence of the nanostructures, may simultaneously contribute to the observed effect. Optimal attachment was observed at a concentration of 1 mM of pFDN (Fig. 4D). This suggested that concentrations higher than 1 mM may cause steric hindrance to cell attachment due to excessive density or that 1 mM nanostructure density is already sufficient given the nucleolin expression level on the cell surface. This result is consistent with previous studies revealing a plateau in cell attachment at higher aptamer concentrations.[43,44] We concluded that the saturation point of this pFDN/HA hybrid hydrogel was approximately 1 mM. Cell proliferation effects of bFGF were validated in HA, mFDN-bFGF/HA, pFDN-NS/HA, and pFDN-bFGF/HA gels after creating pores in the hydrogels *via* freeze–thaw cycles to provide the space for cell growth. On day 1, no significant differences were observed compared with the HA gel (Fig. 4E and F). On day 5, cell proliferation in the pFDN-bFGF/HA gel was significantly higher than that in the mFDN-bFGF/HA and HA gels, showing 1.7- and 2.3-fold increases, respectively.

These DNA sequences and nanostructures-mediated cell behaviors, such as attachment and proliferation, in the pFDN-loaded hydrogels were affected by the physiological stability of the hydrogel matrix and DNA components. To verify this, we evaluated the stability of the HA, mFDN/HA, and pFDN/HA hydrogels under physiological conditions (10% FBS in PBS at 37 °C) (Fig. 4G and Fig. S18). Although the fluorescence intensity of mFDN/HA dramatically disappeared, that of pFDN/HA was maintained until after 4 h of incubation. At 120 h of incubation, the intensity of both hydrogels had mostly disappeared through the degradation of pFDN or bleaching of the fluorescent probe. In addition, over a 120 h incubation period, no significant changes relative to the initial mass were observed among the hydrogels (Fig. S19). The

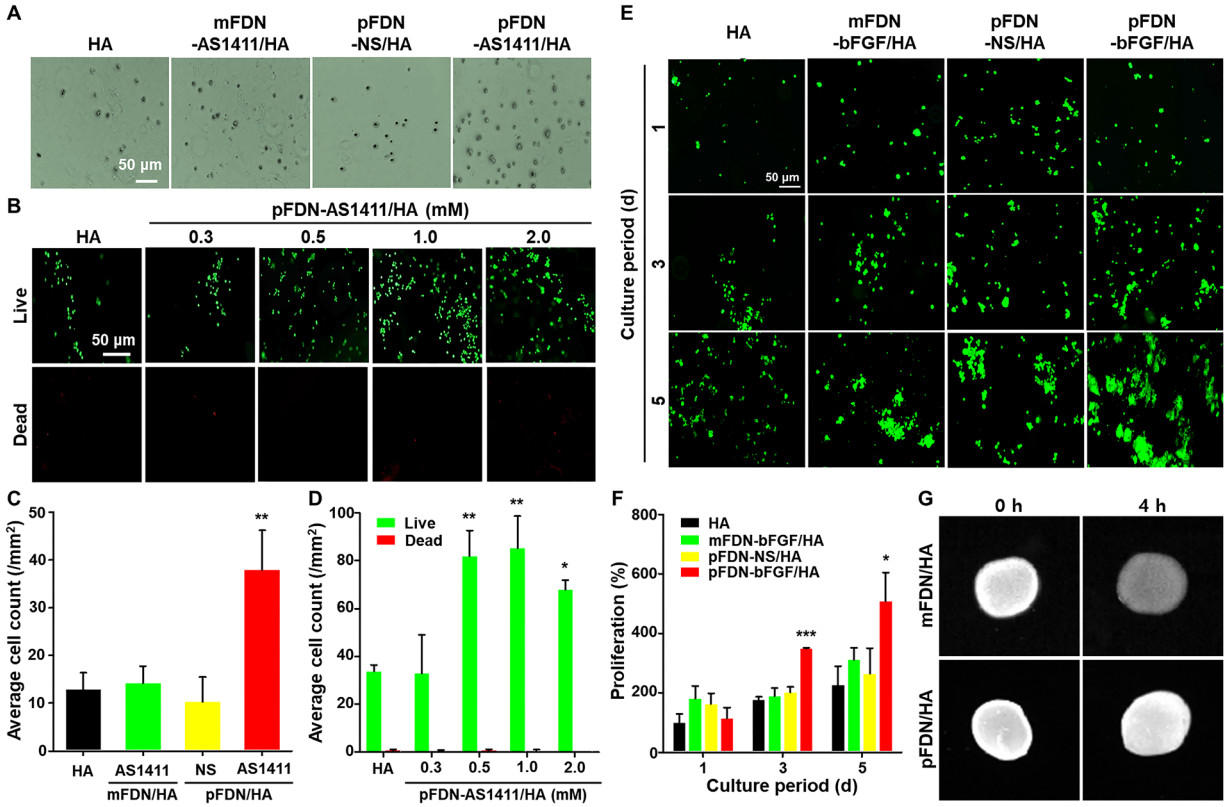

Fig. 4 Evaluation of DNA nanostructures-mediated biological functions on the hydrogel cell culture. (A) OM images of HA, mFDN-AS1411/HA, pFDN-NS/HA, and pFDN-AS1411/HA hydrogels after A-204 cell attachment. (B) CLSM images of HA hydrogels and pFDN-AS1411/HA hydrogels with various FDN concentrations after A-204 cell attachment and staining using the live/dead assay kit. (C) Quantification of attached cells from OM images of HA, mFDN-AS1411/HA, pFDN-NS/HA, and pFDN-AS1411/HA hydrogels. (D) Quantification of attached cells from CLSM images of HA hydrogels and pFDN-AS1411/HA hydrogels with various FDN concentrations. (E) CLSM image of live/dead stained A-204 cells in HA, mFDN-bFGF/HA, pFDN-NS/HA, and pFDN-bFGF/HA hydrogels after 1-, 3-, and 5-d incubation. (F) Proliferation of A-204 cells in HA, mFDN-bFGF/HA, pFDN-NS/HA, and pFDN-bFGF/HA hydrogels after 1-, 3-, and 5-d incubation. (G) Fluorescence image of mFDN/HA and pFDN/HA gels after serum incubation. FDN of each hydrogel is stained with GelRed after serum incubation. Data are presented as the mean ± SD (n = 3); the differences between experimental and control groups were assessed using Scheffe's *post hoc* test. *$p < 0.05$, **$p < 0.01$, and ***$p < 0.001$ *versus* the HA group. OM, optical microscopy; CLSM, confocal laser scanning microscopy; HA, hyaluronic acid; FDN, functional DNA nanostructures; mFDN, monomeric FDN; and pFDN, polymerized FDN.

images captured throughout the observation period demonstrated no discernible morphological alterations in any of the samples. These findings demonstrated that the hydrogels maintained their structural integrity and dimensional stability under physiological conditions, thereby supporting their potential applicability in long-term 3D cell culture systems. Overall, functional DNA nanostructures-mediated effects, enhanced cell attachment and proliferation, were observed within the 3D culture model.

Conclusions

Our results demonstrated the efficiency of incorporating functional DNA nanostructures into methodological approaches. We successfully developed a DNA nanostructure-hydrogel hybrid system based on the polymerization of functional aptamer sequences using RCA. The physicochemical properties of hydrogels remained intact following incorporation of polymerized functional DNA nanostructures, while the nanostructures enabled targeted modulation of cell behaviors. Future research should focus on cellular behavior changes including protein expression, spheroid construction, migration, and differentiation for evaluating the possibility of practical applications. These findings highlight the potential of RCA-generated functional DNA nanostructures as functional components in next-generation biomimetic hydrogels for tissue engineering and regenerative medicine.

Author contributions

Hee Yeon Kim: methodology, investigation, writing – original draft, and visualization. Young Min Kim: methodology, investigation, writing – original draft, and visualization. Keonwook Nam: methodology, investigation, and writing – review and editing. Kyungjik Yang: investigation, writing – review and editing, and visualization. Joohyun Oh: investigation and visualization. Su-Min Han: investigation and visualization. Young Hoon Roh: conceptualization, funding acquisition, writing – review and editing, and supervision.

Conflicts of interest

The authors declare no conflicts of interest.

Data availability

All data are available in the main text and the supplementary information (SI). Supplementary information is available. See DOI: **https://doi.org/10.1039/d5nh00521c**.

Acknowledgements

This research was supported by the National Research Foundation (NRF) grant funded by the Korean government (MSIT) (No. RS-2025-16071710, RS-2025-00517193, and RS-2024-00360849). This research was supported by the Yonsei University Research Fund of 2024 (2024-22-0543). The work was also supported in part by the Brain Korea 21 (BK21) FOUR program.

References

1 A. Roth and T. Singer, The application of 3D cell models to support drug safety assessment: opportunities & challenges, *Adv. Drug Delivery Rev.*, 2014, **69**, 179–189.
2 E. T. Verjans, J. Doijen, W. Luyten, B. Landuyt and L. Schoofs, Three-dimensional cell culture models for anticancer drug screening: Worth the effort?, *J. Cell. Physiol.*, 2018, **233**(4), 2993–3003.
3 Y. Li and K. A. Kilian, Bridging the gap: from 2D cell culture to 3D microengineered extracellular matrices, *Adv. Healthcare Mater.*, 2015, **4**(18), 2780–2796.
4 M. W. Tibbitt and K. S. Anseth, Hydrogels as extracellular matrix mimics for 3D cell culture, *Biotechnol. Bioeng.*, 2009, **103**(4), 655–663.
5 S. Hyung, S. R. Lee, J. Kim, Y. Kim, S. Kim, H. N. Kim and N. L. Jeon, A 3D disease and regeneration model of peripheral nervous system–on–a–chip, *Sci. Adv.*, 2021, **7**(5), eabd9749.
6 S. G. Anthon and K. P. Valente, Vascularization strategies in 3D cell culture models: from scaffold-free models to 3D bioprinting, *Int. J. Mol. Sci.*, 2022, **23**(23), 14582.
7 W. Shin and H. J. Kim, 3D in vitro morphogenesis of human intestinal epithelium in a gut-on-a-chip or a hybrid chip with a cell culture insert, *Nat. Protoc.*, 2022, **17**(3), 910–939.
8 J. Lou and D. J. Mooney, Chemical strategies to engineer hydrogels for cell culture, *Nat. Rev. Chem.*, 2022, **6**(10), 726–744.
9 O. Chaudhuri, Viscoelastic hydrogels for 3D cell culture, *Biomater. Sci.*, 2017, **5**(8), 1480–1490.
10 J. Lou, R. Stowers, S. Nam, Y. Xia and O. Chaudhuri, Stress relaxing hyaluronic acid-collagen hydrogels promote cell spreading, fiber remodeling, and focal adhesion formation in 3D cell culture, *Biomaterials*, 2018, **154**, 213–222.
11 S. Nam, R. Stowers, J. Lou, Y. Xia and O. Chaudhuri, Varying PEG density to control stress relaxation in alginate-PEG hydrogels for 3D cell culture studies, *Biomaterials*, 2019, **200**, 15–24.
12 I. Bružauskaitė, D. Bironaitė, E. Bagdonas and E. Bernotienė, Scaffolds and cells for tissue regeneration: different scaffold pore sizes—different cell effects, *Cytotechnology*, 2016, **68**(3), 355–369.
13 Y. S. Pek, A. C. Wan and J. Y. Ying, The effect of matrix stiffness on mesenchymal stem cell differentiation in a 3D thixotropic gel, *Biomaterials*, 2010, **31**(3), 385–391.
14 G. Benton, I. Arnaoutova, J. George, H. K. Kleinman and J. Koblinski, Matrigel: from discovery and ECM mimicry to assays and models for cancer research, *Adv. Drug Delivery Rev.*, 2014, **79**, 3–18.
15 R. Menezes, R. Vincent, L. Osorno, P. Hu and T. L. Arinzeh, Biomaterials and tissue engineering approaches using glycosaminoglycans for tissue repair: Lessons learned from the native extracellular matrix, *Acta Biomater.*, 2023, **163**, 210–227.
16 T. Wang, C. Chen, L. M. Larcher, R. A. Barrero and R. N. Veedu, Three decades of nucleic acid aptamer technologies: Lessons learned, progress and opportunities on aptamer development, *Biotechnol. Adv.*, 2019, **37**(1), 28–50.
17 A. A. S. Shraim, B. A. Abdel Majeed, M. A. Al-Binni and A. Hunaiti, Therapeutic potential of aptamer–protein interactions, *ACS Pharmacol. Transl. Sci.*, 2022, **5**(12), 1211–1227.
18 S. Yang, H. Li, L. Xu, Z. Deng, W. Han, Y. Liu, W. Jiang and Y. Zu, Oligonucleotide aptamer-mediated precision therapy of hematological malignancies, *Mol. Ther.–Nucleic Acids*, 2018, **13**, 164–175.
19 R. Amano, M. Namekata, M. Horiuchi, M. Saso, T. Yanagisawa, Y. Tanaka, F. I. Ghani, M. Yamamoto and T. Sakamoto, Specific inhibition of FGF5-induced cell proliferation by RNA aptamers, *Sci. Rep.*, 2021, **11**(1), 2976.
20 V. Zlinska, Z. Feketova, A. Czyrek, J. Chudzian, M. L. Zivkovic, V. C. Ursachi, P. Dudeja, B. Fafilek, J. Rynes, G. Rico-Llanos, A. Koudelka, T. Roy, M. Biadun, V. Raskova, K. Svozilova, M. Stroblova, M. Krzyscik, K. Hristova, D. Krowarsch, S. Foldynova-Trantirkova, M. Zakrzewska, L. Trantirek and P. Krejci, Specific inhibition of fibroblast growth factor receptor 1 signaling by a DNA aptamer, *Mol. Ther.–Nucleic Acids*, 2025, **36**(1), 102405.
21 N. Zhao, J. Coyne, L. Abune, P. Shi, X. L. Lian, G. Zhang and Y. Wang, Exogenous signaling molecules released from aptamer-functionalized hydrogels promote the survival of mesenchymal stem cell spheroids, *ACS Appl. Mater. Interfaces*, 2020, **12**(22), 24599–24610.
22 X. Zhang, M. R. Battig, N. Chen, E. R. Gaddes, K. L. Duncan and Y. Wang, Chimeric aptamer–gelatin hydrogels as an extracellular matrix mimic for loading cells and growth factors, *Biomacromolecules*, 2016, **17**(3), 778–787.
23 N. Zhao, M. R. Battig, M. Xu, X. Wang, N. Xiong and Y. Wang, Development of a dual-functional hydrogel using RGD and anti-VEGF aptamer, *Macromol. Biosci.*, 2017, **17**(11), 1700201.
24 E. R. Gaddes, G. Gydush, S. Li, N. Chen, C. Dong and Y. Wang, Aptamer-based polyvalent ligands for regulated cell attachment on the hydrogel surface, *Biomacromolecules*, 2015, **16**(4), 1382–1389.

25 K. Nam, B. I. Im, T. Kim, Y. M. Kim and Y. H. Roh, Anisotropically functionalized aptamer-DNA nanostructures for enhanced cell proliferation and target-specific adhesion in 3D cell cultures, *Biomacromolecules*, 2021, **22**(7), 3138–3147.
26 T. Kim, K. Nam, Y. M. Kim, K. Yang and Y. H. Roh, DNA-assisted smart nanocarriers: progress, challenges, and opportunities, *ACS Nano*, 2021, **15**(2), 1942–1951.
27 C. Yao, R. Zhang, J. Tang and D. Yang, Rolling circle amplification (RCA)-based DNA hydrogel, *Nat. Protoc.*, 2021, **16**(12), 5460–5483.
28 C. Yao, J. Ou, J. Tang and D. Yang, DNA supramolecular assembly on micro/nanointerfaces for bioanalysis, *Acc. Chem. Res.*, 2022, **55**(15), 2043–2054.
29 C. Yao, H. Tang, W. Wu, J. Tang, W. Guo, D. Luo and D. Yang, Double rolling circle amplification generates physically cross-linked DNA network for stem cell fishing, *J. Am. Chem. Soc.*, 2020, **142**(7), 3422–3429.
30 J. Tang, J. Wang, J. Ou, Z. Cui, C. Yao and D. Yang, A DNA/poly-(L-lysine) hydrogel with long shelf-time for 3D cell culture, *Small Methods*, 2024, **8**(7), 2301236.
31 K. Nam, Y. M. Kim, I. Choi, H. S. Han, T. Kim, K. Y. Choi and Y. H. Roh, Crystallinity-tuned ultrasoft polymeric DNA networks for controlled release of anticancer drugs, *J. Controlled Release*, 2023, **355**, 7–17.
32 Y. Lee, K. Nam, Y. M. Kim, K. Yang, Y. Kim, J. W. Oh and Y. H. Roh, Functional polymeric DNA nanostructure-decorated cellulose nanocrystals for targeted and stimuli-responsive drug delivery, *Carbohydr. Polym.*, 2024, **340**, 122270.
33 Y. M. Kim, K. Nam, H. Y. Kim, K. Yang, B. S. Kim, D. Luo and Y. H. Roh, Multifunctional DNA-metal nanohybrids derived from DNA-MgPPi microhybrids by rolling circle amplification, *Small Methods*, 2024, 2401881.
34 K. Lee, T. Kim, Y. M. Kim, K. Yang, I. Choi and Y. H. Roh, Multifunctional DNA nanogels for aptamer-based targeted delivery and stimuli-triggered release of cancer therapeutics, *Macromol. Rapid Commun.*, 2021, **42**(2), 2000457.
35 R. Ueki, S. Atsuta, A. Ueki, J. Hoshiyama, J. Li, Y. Hayashi and S. Sando, DNA aptamer assemblies as fibroblast growth factor mimics and their application in stem cell culture, *Chem. Commun.*, 2019, **55**(18), 2672–2675.
36 J. Hoshiyama, Y. Hayata, A. Eguchi, J. Morimoto, R. Ueki and S. Sando, Analysis of cell signaling profiles induced by DNA aptamer-based FGFR1 agonist, *Anal. Sci.*, 2024, **40**(12), 2251–2258.
37 K. Yang, K. Nam, K. H. Park, H. K. Shin, Y. Kim and Y. H. Roh, Rolling circle replication-based nucleic acid nanostructures for programmable drug delivery, *Nanoscale Horiz.*, 2025, **10**, 3290–3308.
38 Y. H. Roh, R. C. Ruiz, S. Peng, J. B. Lee and D. Luo, Engineering DNA-based functional materials, *Chem. Soc. Rev.*, 2011, **40**(12), 5730–5744.
39 Y. H. Roh, J. H. Park, J. J. Ye, J. E. Lee and D. Luo, Systematic studies of UV stability and photopolymerization efficiency of DNA-based nanomaterials, *Chem. Phys. Chem.*, 2012, **13**(10), 2517–2521.
40 J. B. Lee, Y. H. Roh, S. H. Um, H. Funabashi, W. Cheng, J. J. Cha, P. Kiatwuthinon, D. A. Muller and D. Luo, Multifunctional nanoarchitectures from DNA-based ABC monomers, *Nat. Nanotechnol.*, 2009, **4**(7), 430–436.
41 Y. M. Kim, K. Lee, Y. Lee, K. Yang, D. Choe and Y. H. Roh, Thermoresponsive semi-interpenetrating gelatin-alginate networks for encapsulation and controlled release of scent molecules, *Int. J. Biol. Macromol.*, 2022, **208**, 1096–1105.
42 Y. H. Roh and C. S. Shin, Preparation and characterization of alginate–carrageenan complex films, *J. Appl. Polym. Sci.*, 2006, **99**(6), 3483–3490.
43 N. Chen, Z. Zhang, B. Soontornworajit, J. Zhou and Y. Wang, Cell adhesion on an artificial extracellular matrix using aptamer-functionalized PEG hydrogels, *Biomaterials*, 2012, **33**(5), 1353–1362.
44 E. R. Gaddes, G. Gydush, S. Li, N. Chen, C. Dong and Y. Wang, Aptamer-based polyvalent ligands for regulated cell attachment on the hydrogel surface, *Biomacromolecules*, 2015, **16**(4), 1382–1389.